Available online at www.sciencedirect.com

ScienceDirect

Nuclear Physics A 923 (2014) 31–50

NUCLEAR PHYSICS A

www.elsevier.com/locate/nuclphysa

Simulations of cold nuclear matter at sub-saturation densities

P.A. Giménez Molinelli [a], J.I. Nichols [a], J.A. López [b], C.O. Dorso [a]

[a] *Departamento de Física, Facultad de Ciencias Exactas y Naturales, Universidad de Buenos Aires and IFIBA, CONICET, Ciudad Universitaria, Buenos Aires 1428, Argentina*

[b] *Department of Physics, University of Texas at El Paso, El Paso, TX 79968, USA*

Received 12 November 2013; received in revised form 3 January 2014; accepted 7 January 2014

Available online 10 January 2014

Abstract

Ideal nuclear matter is expected to undergo a first order phase transition at the thermodynamic limit. At such phase transitions the size of density fluctuations (bubbles or droplets) scale with the size of the system. This means that simulations of nuclear matter at sub-saturation densities will inexorably suffer from what is vaguely referred to as "finite size effects". It is usually thought that these finite size effects can be diminished by imposing periodic boundary conditions and making the system large enough, but as we show in this work, that is actually not the case at sub-saturation densities. In this paper we analyze the equilibrium configurations of molecular dynamics simulations of a classical model for symmetric ideal (uncharged) nuclear matter at sub-saturation densities and low temperatures, where phase coexistence is expected at the thermodynamic limit. We show that the most stable configurations in this density range are almost completely determined by artificial aspects of the simulations (i.e. boundary conditions) and can be predicted analytically by surface minimization. This result is very general and is shown to hold true for several well known semi-classical models of nuclear interaction and even for a simple Lennard-Jones potential. Also, in the limit of very large systems, when "small size" effects can be neglected, those equilibrium configurations seem to be restricted to a few structures reminiscent to the "Pasta Phases" expected in Neutron Star matter, but arising from a completely different origin: In Neutron Star matter, the non-homogeneous structures arise from a competition between nuclear and Coulomb interactions while for ideal nuclear matter they emerge from finite (yet not "small") size effects. The role of periodic boundary conditions and finite size effects in Neutron Star matter simulations are reexamined.
© 2014 Elsevier B.V. All rights reserved.

Keywords: Nuclear astrophysics; Nuclear matter phase transition; Molecular dynamics simulations; Finite size effects

E-mail address: pagm@df.uba.ar (P.A. Giménez Molinelli).

0375-9474/$ – see front matter © 2014 Elsevier B.V. All rights reserved.
http://dx.doi.org/10.1016/j.nuclphysa.2014.01.003

1. Introduction

"Nuclear Matter" (NM), an ideal system composed of an infinite number of nucleons which interact through the nuclear potential but not Coulomb, has proved to be an useful theoretical abstraction to study and to characterize the nuclear interaction itself. At sub-saturation densities, NM presents a "liquid–vapor"-like phase transition which has been related to the multifragmentation phenomenon in heavy ion collisions [1].

On the other hand, in the inner crust of Neutron Stars nucleons are expected to exist embedded in a degenerate electron gas and at sub-saturation densities. This prompted the definition of "Neutron Star" Matter (NSM) as a charge-neutral system of nucleons and electrons (which exactly balance the charge of the protons). The study of NSM at sub-saturation densities is important for a variety of topics which include several phenomena related to heavy ion reactions, the symmetry energy term in the nuclear EOS, the structure of neutron star crusts, etc. Pioneering studies on NSM based on the compressible liquid drop model [2,3], Hartree–Fock method [4], and energy minimization techniques [5,6] showed that transitions from spherical nuclei to "nuclei" shaped as rods and slabs, which are collectively named "Pasta Phases", are to be expected in cold NSM at sub-saturation densities. For NM, however, at those same densities, coexistence between a liquid-like and a vapor-like phase is expected to exist. More recent investigations [5–17] have used dynamical methods to study such transitions in NSM. In the previous studies listed, the Coulomb interaction has been approximated either by using a Wigner–Seitz cell [5], assuming uniform electric charge densities [6], Thomas–Fermi screened Coulomb potential (see, e.g. [11]) or by an Ewald summation [19]. Dynamical simulations of NSM under periodic boundary conditions at low temperatures ($T \lesssim 1$ MeV) indeed show that nucleons self-assemble into pasta-like objects: mainly "gnocchi", "spaghetti", "lasagna" and their bubble counterparts. The issue of "finite size" effects affecting the results of NSM simulations arises occasionally, in particular when a given model yields only one structure per simulation cell (see for example [20]), but it is systematically accepted that they would disappear if the system is made large enough.

In NSM, Coulomb interaction is an essential ingredient for the formation of the pasta-like structures. Williams and Koonin [6], for instance, explained the transitions between different "nuclei" topologies in terms of a competition between a short-range nuclear surface energy, which becomes minimized through aggregation, and a long-range Coulomb energy which gets reduced by an opposite dispersion. More recent studies of Horowitz and coworkers [18] re-examine this assertion as an example of frustration, a phenomenon that emerges from the impossibility to simultaneously minimize all interactions.

However, unbeknownst to many, similar structures have been found to be stable solutions in simulations of Lennard-Jones fluids without any Coulomb interaction [39]. For the Lennard-Jones fluid, those structures occur in the density region that corresponds to phase coexistence at the thermodynamic limit, and since only one gnocchi, spaghetti or lasagna per simulation cell exists the author argues that "finite size" effects are responsible for their formation. Given the similarities between the Lennard-Jones potential and the Nuclear Interaction (short-ranged and attractive), the same situation is expected in NM simulations.

Recapitulating, when Coulomb interaction is included in a simulation, inhomogeneous solutions are explained as resulting from a competition between the short-ranged attractive nuclear part of the interaction and the long-ranged Coulomb potential. But when only short-ranged attractive interactions are present (or when a model yields only one structure per cell), the existence of equilibrium non-homogeneous structures is attributed to non-specific "finite size" (or interfacial)

effects. We find it interesting and suggestive that the shapes of the possible equilibrium configurations are so similar even if their origin and scale is completely different.

The main focus of this paper is the study of the role of finite size and periodic boundary conditions in the determination of the solutions in simulations of ideal NM as a first step to estimate the extent to which they persist in NSM simulations. We use the same model that we already used in [16] to simulate NSM but this time without any form of Coulomb interaction, as a model of NM.

The approach to be followed is a combination of classical molecular dynamics of large (but finite) systems under periodic boundary conditions, topological analysis tools and analytical geometrical considerations. In Section 2 the classical molecular dynamics model used will be briefly reviewed for completeness. The reader is encouraged to review the extensive list of references provided to assess the fitness of the model for this and more general, realistic, purposes. Also, since the main focus of this work is set on the general conditions of the numerical simulations rather than on the details of the physical model, we performed simulations with several popular semi-classical interaction models of nuclear interaction and also with a simple Lennard-Jones potential. Section 3.1 presents a detailed study of the equilibrium configurations of ideal symmetric nuclear matter with medium compressibility, followed in Section 3.2 by similar studies with other two potentials that have been successfully used in the past to study nuclear-like systems. The specific role of finite size effects and boundary conditions is thoroughly discussed in Section 4, and a summary of the main results is presented in Section 5 along with some concluding remarks. Visual representations of simulated systems where made using VMD [21].

2. Classical molecular dynamics

This work uses a classical molecular dynamics model (CMD) to study infinite nuclear matter at low temperatures and sub-saturation densities.

The trajectories of the nucleons are governed by classical equations of motion dictated by forces produced by the Pandharipande [23] potentials:

$$\begin{aligned} V_{np}(r) &= V_r\big[\exp(-\mu_r r)/r - \exp(-\mu_r r_c)/r_c\big] \\ &\quad - V_a\big[\exp(-\mu_a r)/r - \exp(-\mu_a r_c)/r_c\big], \\ V_{nn}(r) &= V_0\big[\exp(-\mu_0 r)/r - \exp(-\mu_0 r_c)/r_c\big], \end{aligned}$$

where V_{np} is an attractive potential between a neutron and a proton and V_{nn} is a repulsive interaction between similar nucleons (nn or pp); both are cut off at a radius of $r_c = 5.4$ fm, after which the potentials are set to zero. The Yukawa parameters μ_r, μ_a and μ_0 were phenomenologically adjusted by Pandharipande to yield a saturation density of $\rho_0 = 0.16$ fm^{-3}, a binding energy $E(\rho_0) = 16$ MeV/nucleon and a compressibility (actually, bulk modulus) listed by the original authors in [23] as 250 MeV for the "Medium" model, and 535 MeV for the "Stiff" [23]. Even if the Stiff compressibility is rather higher than the accepted value of 240 ± 30 MeV [35–37], the fact that it qualitatively reproduces many aspects of real nuclear systems [23,30] indicates that the model captures the essential physics of the nuclear interaction and thus makes it adequate for the current purposes. The same is true for the SSP model described in Section 3.2.1. Furthermore, comparing models with different compressibilities allows us to examine the dependency (or lack thereof) of the phenomenology on the compressibility.

The trajectories of all nucleons are obtained by solving the classical equations of motion using a symplectic Verlet algorithm with energy conservation of $\mathcal{O}(0.01\%)$. Systems, of $A = 1728$ to

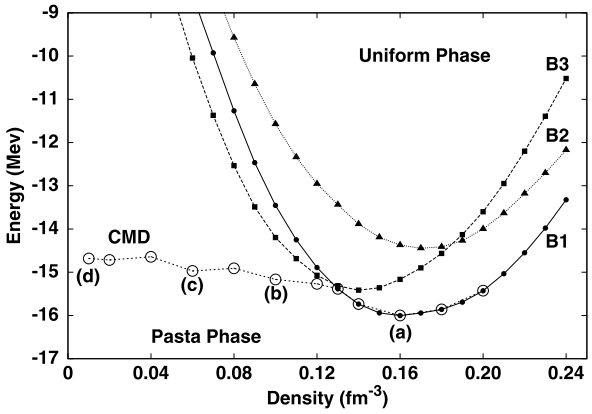


Fig. 1. Binding energy per nucleon for systems obtained with the Pandharipande medium potential with simple cubic (B1), body centered cubic (B2) and diamond (B3) crystal lattices, and using molecular dynamics (CMD) at $T = 0.001$ MeV (CMD). The structures corresponding to the four labeled points ((a) through (d)) are shown in Fig. 2. Notice that around saturation density the CMD results agree with those of the simple cubic lattice.

$A = 46\,656$ nucleons and densities in the range of $0.01\ \text{fm}^{-3} \leqslant \rho \leqslant 1.25\rho_0$ are simulated in cubic cells under periodic boundary conditions. For simplicity only isospin symmetric matter $x = z/A = 0.5$ was studied. To control the temperature, the Andersen thermostat [38] was used.

Perhaps the most evident drawback of the model is its lack of explicit quantum features. By making interactions between like nucleons purely repulsive, its authors meant to include some Pauli repulsion-like effects that account for the instability of pure neutron matter within the model, but little more. It should be understood that, as such, classical models are meant to provide a transparent classical framework to some properties and phenomenology of nuclear matter and not to give a quantitatively accurate description of every aspect of the nuclear interaction. The use of classical molecular dynamics to study nuclear reactions was pioneered by Wilets and coworkers [22] and advanced by Pandharipande [23] and others [24–26] who attempted to include Pauli effects *via* momentum dependent potentials. In particular, the model used in this work has a rich and fruitful history in the study of heavy ion collisions [30–34].

More recently, classical molecular dynamics models have been used to study cold nuclear matter in conditions relevant for the study of neutron star crusts [18,27–29]; in particular the CMD model has been adapted by some of us to study nuclear systems under such conditions [16,17]. And while their use to study nuclear matter at low energies is difficult to justify *a priori*, results previously obtained with this models are in very good agreement with those yielded by more quantum-like dynamical models [16,14] and even quantum mean field calculations [20], in regard to the description of the Pasta phases. Moreover, their simplicity can put them at an advantage over other models at providing global information about phase transitions, where the details of the interactions are often of little importance.

The procedure we follow is twofold. To study the uniform phase at zero temperature, a crystalline structure at a given density is constructed and its energy per nucleon calculated by direct summation between all nucleons. The dependence of the binding energy of the uniform phase on the density is explored by scaling the lattice parameter. This yields the energy versus density curve shown in Fig. 1. This procedure, identical to the one used by Pandharipande [23], produces the characteristic U-shaped curve, with a minimum at the saturation or normal nuclear density.

Pandharipande et al. assumed that the nucleons in the ground state were arranged as a simple cubic lattice for the whole range of densities, but that is not necessarily the case for every model of nuclear interaction, as we shall see in Section 3.2. Given that nuclear matter is composed of two kinds of particles (neutrons and protons), the crystal geometries they adopt are similar to those formed by binary alloys. As we will see, the relevant crystal structures for the studied cases are the B1 (a simple cubic lattice in which every first neighbor of a proton is a neutron and *vice versa*), the B2 (a BCC lattice), and the B3 (a diamond lattice with nucleons arranged so that every first neighbor of a protons is a neutron and *vice versa*).

At densities around and below the saturation one we also perform CMD simulations starting from a random positioning of nucleons in a cubic cell under periodic boundary conditions. Initial velocities are taken from a Maxwell–Boltzmann velocity distribution corresponding to a given initial temperature. The systems are evolved until equilibrium is achieved at a high temperature ($T \gtrsim 2$ MeV) and then brought down to the final desired temperature using the Andersen thermostat in small temperature steps. After reaching equilibrium, the analysis tools described in [17] were used to characterize and visualize the produced configurations.

3. MD calculations

3.1. Medium compressibility matter

Fig. 1 shows the near zero temperature results for symmetric ($x = 0.5$) matter interacting through the Pandharipande medium potential (see figure caption for details). As can be seen, CMD reproduces the simple cubic (B1) lattice calculations, corresponding to the uniform phase, up to a density of $\rho \approx 0.13$ fm^{-3}, while for lower densities the systems goes into a series of non-homogeneous phases. Also shown in Fig. 1 are the energies expected for a uniform body centered cubic (B2) and diamond (B3) lattice structures which, being higher in energy, do not correspond to the $T = 0$ case. Fig. 2 shows visual representations of the structures corresponding to the four densities labeled from (a) to (d) in Fig. 1.

Before we continue, we deem it necessary to advocate for the correctness of these results, since when we first found them we disregarded them as wrong because of well established prejudices. The structures of Fig. 2 resemble those Ravenhall obtained [5] using a liquid drop model with Coulomb interaction in the Wigner–Seitz approximation. Ever since then, in the context of nuclear systems, the formation of non-homogeneous arrangement of nucleons has always been attributed to the competition between nuclear and Coulomb energies. When we found the same structures without Coulomb interaction we were naturally surprised and skeptical about our results, but they are correct and had actually been found recently by other author in a different context. In [39], grand canonical Monte Carlo simulations of a Lennard-Jones fluid are carried out in the density region that corresponds to the liquid–vapor coexistence region at the thermodynamic limit. The author finds the same set of non-homogeneous structures that we found for ideal nuclear matter and argue that they are stabilized by "finite size effects", related to interfacial energies that would vanish in the limit of infinite system size. As we shall prove in Section 4, that is not entirely true. At these densities and temperatures, those structures are the correct solution for simulations of systems of any size under periodic boundary conditions, given that only short-ranged attractive potentials are present.

For now, lets return to the analysis of out results for CMD with the medium potential. The B1 curve of Fig. 1 can be used to perform a polynomial fit around its minimum to extract an analytic expression, which can then be used to calculate the compressibility around the saturation density

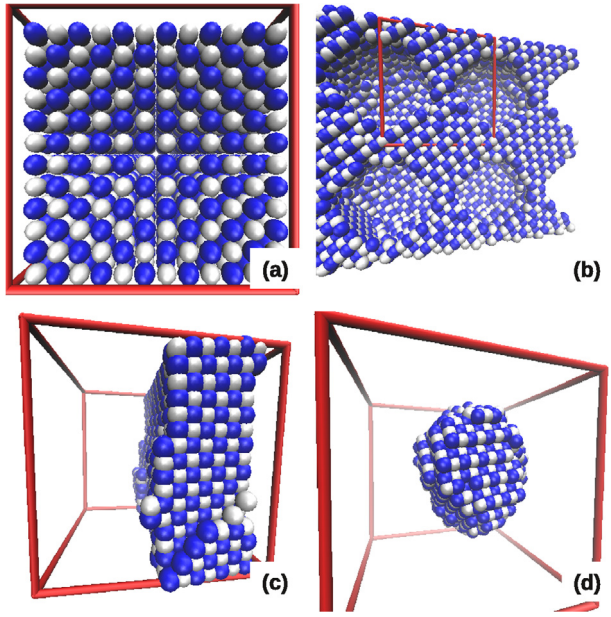


Fig. 2. (Color online.) Structures produced by CMD, corresponding to the labeled points of Fig. 1. Point A corresponds to a regular (B1) lattice, while the rest of the points are non-homogeneous structures.

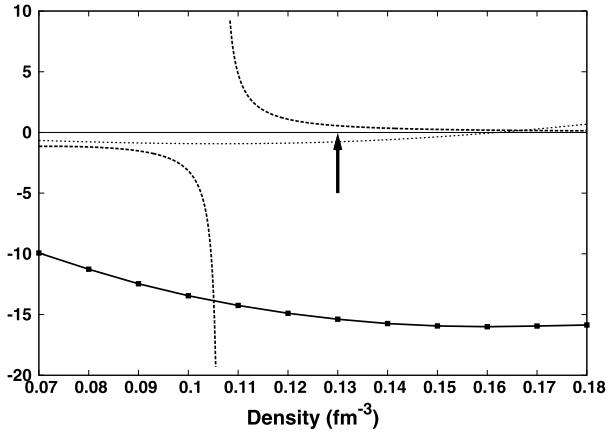


Fig. 3. Energy (full lines with squares), pressure (dashed line) and compressibility (dotted line) for the uniform B1 lattice of the medium potential. The arrow points at the density at which the simulated systems departs from homogeneity.

through $K = 9\rho_0^2[d^2(E/A)/d\rho^2]_{\rho_0}$. Fitting with a degree two polynomial, the bulk modulus for the medium Pandharipande potential is found to be 283 MeV, comparable with the value of 250 MeV quoted by its creators, who used different fitting polynomial.

In Fig. 3, we plot the energy, pressure and compressibility for the homogeneous B1 lattice of Pandharipande's medium potential. The pasta-like structures are found in a mechanically unstable (negative pressure) density region, but well above the divergence in compressibility that would signal the thermodynamic instability. This enhancement of the stability region for the

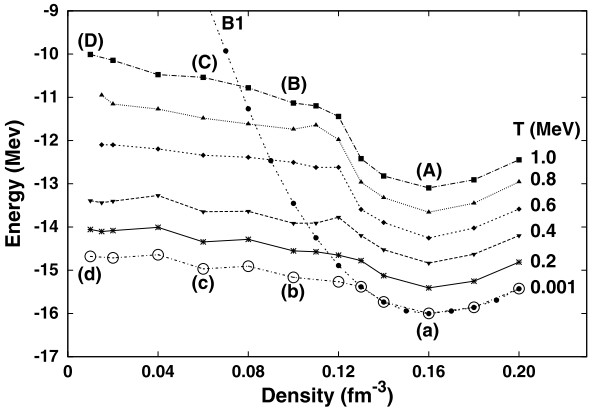


Fig. 4. Binding energy per nucleon for systems obtained with the Pandharipande medium potential at the listed temperatures.

homogeneous phase had already been observed for a Lennard-Jones system in [39]. As we shall discuss in Section 4, this is produced by the imposition of periodic boundary conditions.

Continuing with the study at higher temperatures, Fig. 4 shows the same type of results as Fig. 1 for temperatures $0.001\ \text{MeV} \leqslant T \leqslant 1.0\ \text{MeV}$. As it can be seen in the figure, at densities $\rho \gtrsim 0.13\ \text{fm}^{-3}$ and at all of these temperatures the curves follow the "U" shape characteristic of the uniform $T = 0$ crystalline phase. As in the case of zero temperature, if the density decreases below $\rho \sim 0.13\ \text{fm}^{-3}$ the systems again move away from the uniform phase forming non-homogeneous stable arrangements. Fig. 5 shows the structures obtained for the highest temperature studied ($T = 1.0$ MeV) for the four densities labeled from "a" to "d" in Fig. 4.

These non-homogeneous structures being formed in the low density region can be characterized using the mean curvature and Euler number. As explained in detail in [17], different structures have distinct values of these variables and, in general, follow the pattern outlined in Table 1; as a reference, the perfect crystals formed at $T = 0$ and $\rho \gtrsim 0.13\ \text{fm}^{-3}$ (e.g. point "A" in Figs. 1 and 4) are formally uniform and infinite because of the periodic boundary conditions imposed, hence they have no surfaces and null Euler characteristic.

The curvature-Euler coordinates of the labeled structures of Fig. 4 are presented in Fig. 6; points joined by lines all have the same densities but their temperatures vary through $T = 0.001, 0.1, 0.5, 0.6, 0.8$ and 1.0 MeV with the letter labels corresponding to those of Fig. 4. Again, the cases "A–a" at normal density (ρ_0) correspond to uniform crystalline structures so all have zero curvature and Euler number at the temperatures studied. In the case "B–b" of density $0.1\ \text{fm}^{-3}$ the almost spherical bubbles at $T = 0.001$ MeV become distorted at higher temperatures. Perhaps the most interesting case is "C–c" at $\rho = 0.06\ \text{fm}^{-3}$, which goes from being a perfect "lasagna" to a "jungle-gym", a complex of lasagna joined by columns (and similar to the Schwarz's Primitive surface of differential geometry). Structures "D–d", on the other side, go from spherical "gnocchi" to deformed droplets. In any case, they clearly do not correspond to the mixed phase one expects in the thermodynamic limit. This behavior is usually attributed to "finite size", generally implying "small size". However, as we shall see in Section 4 this behavior does not vanish in the $L \to \infty$ limit.

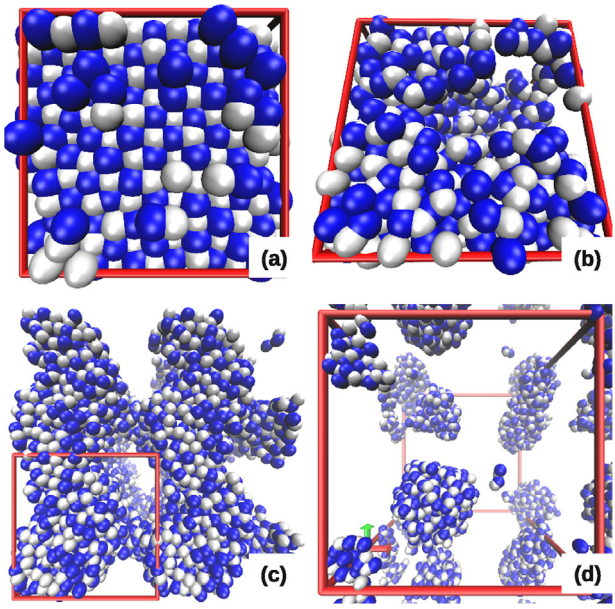


Fig. 5. (Color online.) Structures corresponding to the labeled points of Fig. 4 obtained with the Pandharipande medium potential at $T = 1.0$ MeV.

Table 1
Classification curvature-Euler.

	Curvature < 0	Curvature ~ 0	Curvature > 0
Euler > 0	Anti-Gnocchi		Gnocchi
Euler ~ 0	Anti-Spaghetti	Lasagna	Spaghetti
Euler < 0	Anti-Jungle Gym		Jungle Gym

3.2. Higher compressibility potentials

To check whether the comportment presented in the previous section is potential-dependent, it is instructive to repeat the study using other models to extract generalities of the behavior of NM simulations at low temperature and sub-saturation densities and under periodic boundary conditions. In particular, we use potentials with higher values of the compressibility that have been successfully used in the past to study heavy ion collisions or NSM.

3.2.1. A simple semi-classical potential

A higher compressibility set of potentials that has been used for a variety of studies of nuclear matter [27–29] is the one described by its creators [18] as a "simple semi-classical potential" (SSP). In summary, the SSP is composed of:

$$V_{np}(r) = ae^{-r^2/\Lambda} + [b - c]e^{-r^2/2\Lambda},$$
$$V_{NN}(r) = ae^{-r^2/\Lambda} + [b + c]e^{-r^2/2\Lambda},$$

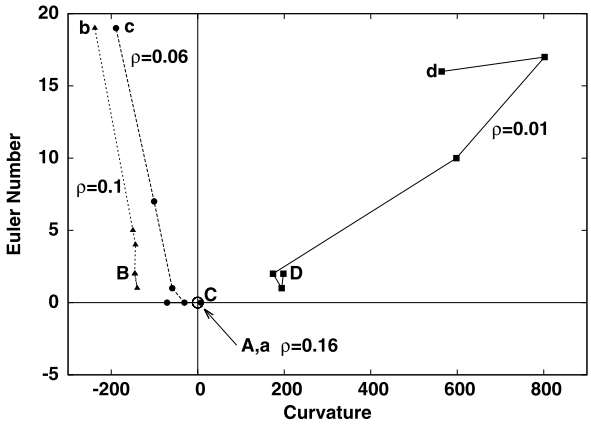


Fig. 6. Curvature-Euler coordinates of the structures from Fig. 4. The lines connect points with the same densities but temperatures varying from $T = 0.001$ MeV to 1.0 MeV.

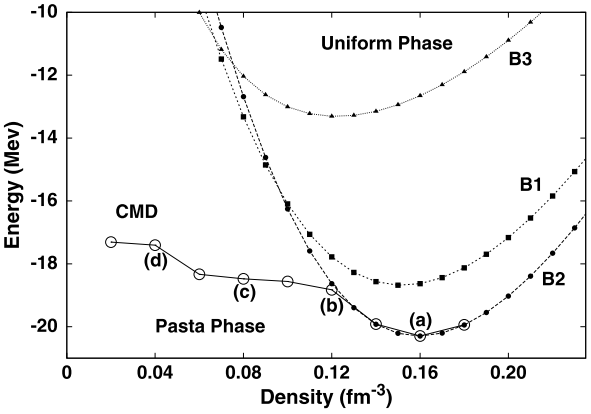


Fig. 7. Binding energy per nucleon for systems obtained with the Simple Semi-classical Potentials for crystalline lattices with B1, B2 and B3 lattice geometries, and using molecular dynamics at $T = 0.001$ MeV (CMD). The structures corresponding to the four labeled points ((a) through (d)) are shown in Fig. 8.

where, again, the potential between a neutron and a proton is attractive, and that between like particles is repulsive. The parameters a, b, c, and Λ have been adjusted so to adequately reproduce binding energies of ions and NM properties such as saturation density and energy.

Fig. 7 shows the binding energies per nucleon obtained from symmetric systems constructed with the SSP in crystalline lattices with B1, B2 and B3 crystal geometries. When used in our molecular dynamics code at $T = 0.001$ MeV – and without the Coulomb potential – the SSP produces structures with the energies labeled in Fig. 7 as CMD. Interestingly, at saturation density this potential produces a B2 crystal instead of the B1 produced by the lower compressibility model used in Section 3.1.

The "normal" density point of this potential is at the correct value (i.e. at $\rho = 0.16$ fm^{-3}) but at the slightly lower binding energy of -20.3 MeV. Again, using a polynomial fit to the bottom part of the "U" of the B2 curve of Fig. 7, allows us to extract a value of the compressibility of the order of 418 MeV, much higher than the value of the Pandharipande medium potential.

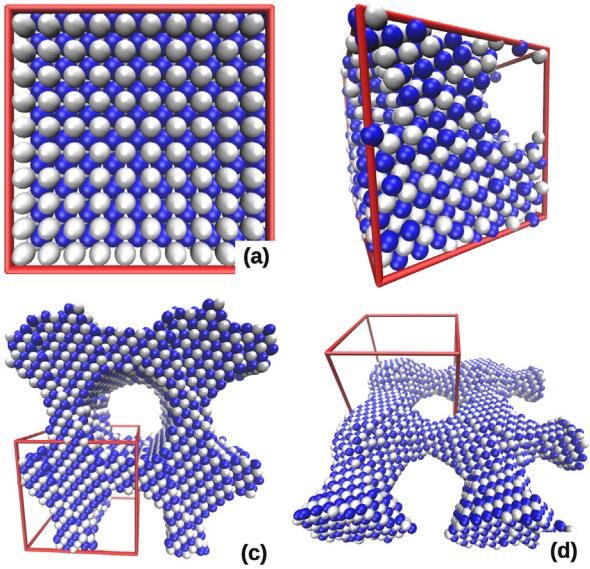


Fig. 8. (Color online.) Structures obtained with the SSP corresponding to the labeled points of Fig. 7. Points (a) and (b) correspond a regular lattice uniform phase, while the other points are again pasta-like structures. The structure of panel (d) appeared for the medium potential as well and is discussed in Section 4.

As in the case of the medium Pandharipande potential, at densities $\rho \gtrsim 0.12$ fm^{-3} the CMD results agree with the lowest-energy crystalline structure, which in this case is the B2, and at lower densities the systems form pasta-like objects. The structures corresponding to the four labeled points ("a" through "d") are shown in Fig. 8.

Except for minor differences, the scenario that the SSP presents is very similar to that obtained with the Pandharipande medium potential. Namely, it is possible to obtain pasta-like structures in SSP simulations of cold temperatures at sub-saturation densities and periodic boundary conditions, even without the disrupting effect of the Coulomb interaction.

3.2.2. Stiff Pandharipande potential

The same calculations are now repeated for the stiff version of the Pandharipande potential, see [23]. This interaction produces the E/A versus ρ shown in Fig. 9 for symmetric nuclear matter and zero temperature in B1 and B3 crystals for different density ranges; the B2 structure produced energies higher than the scale of the figure. Also presented are the binding energies of the structures obtained with CMD at $T = 0.001$ MeV.

In this case the saturation point for cold matter occurs at $\rho = 0.15$ fm^{-3}, with an energy of 16.5 MeV and for a B3 structure. The authors of the potential did not realize that the lowest energy geometry was a B3 lattice and assumed a B1 structure for the whole range of densities in their estimation of the compressibility. This led to an incorrect value. Using a polynomial fit of the B3 curve to estimate the compressibility at the true saturation point, as done with the other two potentials, yields a value of about 494 MeV, somewhat smaller than the value of 535 MeV that Pandharipande obtained using a B1 lattice [23].

Furthermore, at a density of about 0.17 fm^{-3}, this potential presents a solid-solid phase transition between B1 and B3 structures. The CMD simulations correctly show that at $\rho \gtrsim$ 0.17 MeV the preferred crystalline structure is the B1, while for lower densities in the range

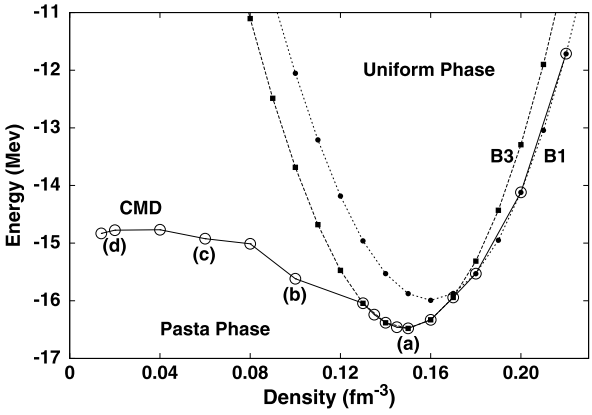


Fig. 9. Binding energy per nucleon for systems obtained with the Pandharipande stiff potential for crystalline lattices with B1 and B3 crystal geometries, and using molecular dynamics at $T = 0.001$ MeV (CMD). The structures corresponding to the four labeled points ((a) through (d)) are shown in Fig. 10.

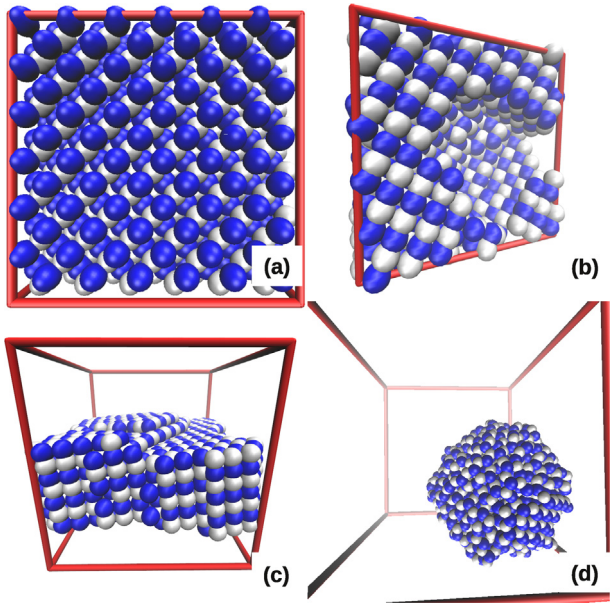


Fig. 10. (Color online.) Structures corresponding to the labeled points of Fig. 9. Again, point a corresponds to the uniform phase, while points b through d are pasta-like structures.

$0.13 \lesssim \rho \lesssim 0.17$ fm^{-3} it is B3. The departure from the homogeneous phase into the pasta-like structures starts at densities smaller than $\rho \approx 0.13$ fm^{-3}; the structures corresponding to the four labeled points ("A" through "D") are shown in Fig. 10.

Again, except for minor differences, ideal stiff nuclear matter also produces pasta-like formations at cold temperatures and sub-saturation densities without any Coulomb interaction. The fact that different, but qualitatively similar, interaction potentials produce pasta-like structures at sub-saturation densities in absence of Coulomb interactions suggests that the existence of these

structures is due to the general conditions of the simulations (i.e. finite size, low temperature and artificial periodicity) rather than to the particulars of the model.

4. Finite size effects and periodic boundary conditions

Historically the existence of pasta phases in NSM has been attributed to the competition between surface and Coulomb energies. While the short-ranged attractive nuclear interaction drives the system to a minimum surface configuration, the long-ranged repulsive Coulomb interaction drives protons as far away from each other as possible. The competition is settled by producing the non-homogeneous pasta structures. Whenever only one structure per cell is observed in a model that includes Coulomb interaction, the authors warn that vaguely defined "finite size effects" might be in action [8,13,20]. Those finite size effects themselves have never been studied in detail, to our knowledge. As we have seen in the previous sections and from studies by other authors [39], in both molecular dynamics or Monte Carlo simulations under periodic boundary conditions those finite size effects can somehow produce one pasta-like structure with Lennard-Jones-like potentials only, without Coulomb interaction.

To elucidate the origin of these Coulomb-less pasta-like structures, this section will first demonstrate that such structures exist indeed irrespectively of the details of the potential, as long as the pair-wise potential is short-ranged and attractive. We will then proceed to study some geometrical and size-related aspects of the simulations which appear to bear a large share of the responsibility for the formation of these structures, i.e. we will study how the "finite size effects" themselves produce and stabilize these structures.

4.1. Lennard-Jones "pasta"

Pasta, as expected to exist in neutron star crusts, originates from the competition between short-range attractive nuclear interaction and long-range Coulomb repulsion. Due to such proposed origin, pasta structures were not expected to exist in pure nuclear matter but, as seen in the previous sections, they indeed appear in simulations. All the semi-classical nuclear potentials we used consist of an attractive part acting on nucleons of different isospin and a repulsive part acting on identical nucleons, both of the same range. Before we learned of the results in [39], to discard the possibility that the pasta-like structures were being shaped by the competition between this two parts of the interaction, we decided to simplify the system treated down to a simple one-component, one-potential system.

We adapted CMD to perform simulations using a simple Lennard-Jones (LJ) potential under the same conditions of temperature and system sizes as those for the nuclear case. The interaction potential between any two particles is given by

$$V_{\mathrm{LJ}}(r) = 4\epsilon\left[\left(\frac{\sigma}{r}\right)^{12} - \left(\frac{\sigma}{r}\right)^{6}\right],$$

with σ and ϵ chosen to have the minimum energy in -16 in arbitrary units and at $\rho = 0.16$, similar to those of the Pandharipande medium potential used in Section 3.1, but in a close-packed lattice (the preferred for this potential).

Fig. 11 shows some of structures obtained with the LJ potential, similar to those found for nuclear matter. Since the formation of the same pasta-like structures had also been observed in grand canonical Monte Carlo simulations LJ systems [39], these structures do not result from faulty dynamics or equilibration, as we feared the first time we saw them. Furthermore, given that

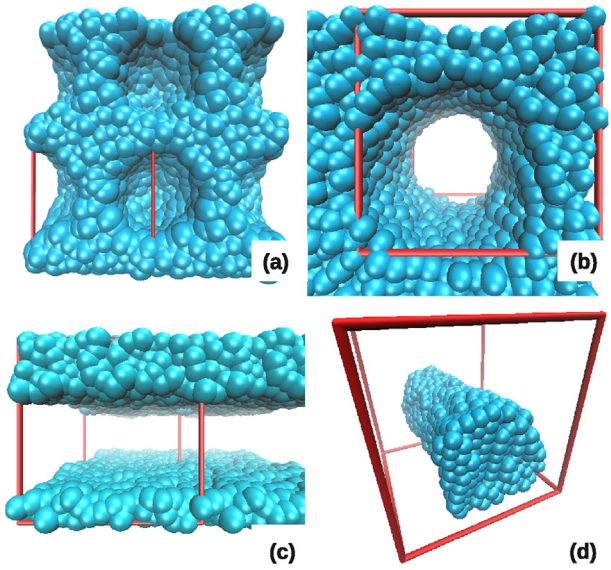


Fig. 11. (Color online.) Structures obtained with a Lennard-Jones potential.

there is no attractive–repulsive interplay of forces in a one component LJ fluid, and the dynamics seem irrelevant, these pasta-like structures can only arise from common geometrical features our simulations and those of [39]. As such, they present the perfect scenario to study in detail the role of finite size and boundary conditions, which we do in the following section.

4.2. Geometric considerations

A recurrent question of numerical calculations is the validity of the results given the finite size of the systems actually treated. For uniform systems, this concern is addressed by imposing periodic boundary conditions on a cell much larger than the range of the inter-particle potential. At fixed volume, this practice enables one to accurately simulate systems which are homogeneous in scales smaller than that of the cell. Yet, no matter how large, the systems simulated this way are still finite. Because of this, periodic boundary conditions limit the maximum density fluctuations wave-lengths to the size of the simulation cell. This is a serious drawback at the so-called "spinodal" region, where mean field theories predict phase coexistence and density fluctuations of every possible length are expected. In addition, periodic boundary conditions also break the isotropy of the radial correlation function [40]. While these issues are not a serious drawback for homogeneous media, simulations of non-homogeneous systems may be heavily biased by the artificial periodicity. A first glimpse of this fact is the extension of the stability region for the uniform phase observed in Section 3.1.

A characteristic worth investigating is that in all of the pasta-like structures obtained both with ideal nuclear matter (cf. Figs. 2, 5, 8 and 10) and with a LJ medium (Fig. 11) only one structure appears to be formed in each cell, independent of the cell size. The structures seem to be limited to one spherical drop, one rod, one slab, one cylindrical tube or one spherical bubble per cell, except at densities during transitions. Since the LJ potential is short-ranged and attractive, the only contributions to energy of the non-homogeneous structures arise from bulk and surface terms, and perhaps curvature. The same is true for isospin symmetrical NM simulations. And at low

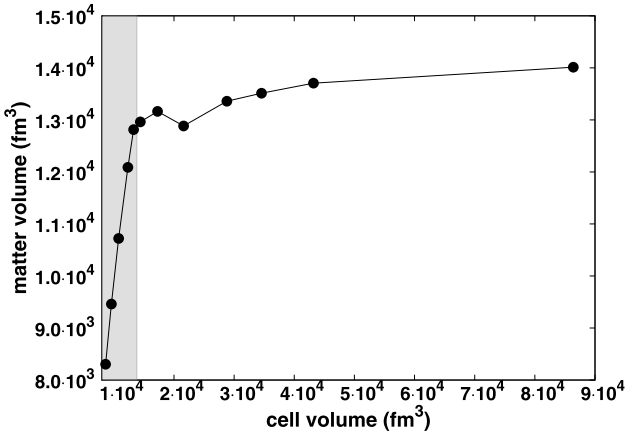


Fig. 12. Volume occupied by matter vs. cell's volume for the medium Pandharipande potential. Points in the shaded area correspond to uniform states at densities from 0.2 fm^{-3} to 0.13 fm^{-3}. The rest correspond to non-homogeneous configurations at densities between 0.12 fm^{-3} and 0.02 fm^{-3}.

enough temperature, the most stable configuration is that of minimum energy. In this scenario, that is achieved maximizing volume while minimizing surface (and eventually curvature).

To examine the results from the simulations under the light of this observation, we turn to study the volume and surface of structures obtained at zero temperature with the medium compressibility potential of Section 3.1.

In our simulations at zero temperature the number of particles is fixed and the cell volume is adjusted to yield the desired density. The total volume occupied by the nucleons can be evaluated by the digitalization process described in [17]. As it can be seen from Fig. 12, in the range of densities studied, the total cell volume increases ten times while the volume occupied by nucleons in the non-homogeneous configurations varies less than 10%. In other words, as the pasta-like structures change from drops to rods, slabs, etc. the total volume occupied by nucleons remains practically constant. This indicates that the bulk (volume) energy term is almost constant even when the shapes change, and that points to the surface energy as the critical factor in determining which specific structure is the most stable for a given density.

To quantify the variation of the surface area of the structures in terms of the cell size we perform a simple geometric exercise (which we later found out had already been done in [7] but with other objective). We calculated the surface area of simple shapes (spherical drop, cylindrical rod, slab and their bubble counterparts) and plot it as a function of the fraction of the cubic cell's volume they occupy, u.

Each pasta-like shape can be characterized by its volume and surface area, which in turn can be parametrized in terms of the cubic cell's side L and a characteristic length a, namely the radius of a spherical drop, cylindrical rod, the width of a lasagna slab, etc.

It must be remembered that for finite systems with periodic boundary conditions the simulation cell imposes some constrains. Due to periodic boundary conditions, "surfaces" attached to the faces of the simulation cell are effectively bulk. Both slabs and cylindrical rods or bubbles have some faces attached to the surfaces of the cubic cell in which they are inscribed. Since these lateral faces are not true surfaces they should not be taken into account.

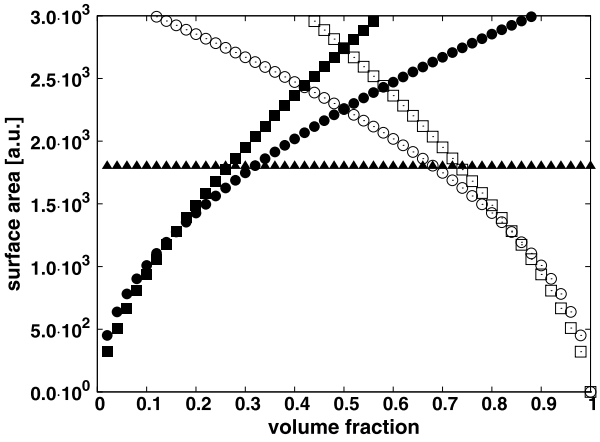


Fig. 13. Surface area of various simple shapes as a function of volume fraction for a cell of $L = 30$. The shapes are: spherical drop (full squares), cylindrical rod (full circles), slab (full triangles), cylindrical bubble (empty circles) and spherical bubble (empty squares).

In this way, the effective surface area of each shape (sphere, rod or slab) can be written in terms of a and the cubic cell's length L. Then its variation with the volume fraction u can be studied. The surface area of a single shape per cell as a function of L and u is found to be

$$S_{sphere} = 4\pi\left(\frac{3}{4\pi}\right)^{\frac{2}{3}} \times u^{\frac{2}{3}} \times L^2,$$

$$S_{rod} = 2(\pi)^{\frac{1}{3}} \times u^{\frac{1}{3}} \times L^2,$$

$$S_{slab} = 2 \times L^2.$$

The bubble counterparts have similar expressions with u replaced by $(1 - u)$.

Since the surface areas of all shapes studied scale as L^2, the specific shape that has the least surface area for a given volume fraction is independent of system size L. Then this effect does not vanish in the limit $L \to \infty$, as it is generally implied when "finite size" effect are invoked.

Fig. 13 shows these surfaces as a function of the volume fraction.

In order of increasing volume fraction, the preferred shape (that of least surface area) goes from spherical drop, to cylindrical rod, to slab, to cylindrical bubble and finally to spherical bubble. Notably, these are the same structures found in almost every study of nuclear pasta, and in the same order, but arising solely from surface minimization under periodic boundary conditions.

For systems without long range interactions this schematic result should be exact for large enough systems, i.e. for cell sizes much larger than the range of the interaction potential, where interfacial and curvature effects can be truly neglected. Of course, in order to determine the most stable configuration one should be able to parametrize every possible surface with the periodicity of the cell and then find which one is minimal for any density.

Fig. 14, shows configurations found with Pandharipande's medium potential at $T = 0.1$ MeV and $\rho = 0.04$ fm^{-3} and 0.08 fm^{-3} for two system sizes: $A = 1728$ and $A = 4096$. It is clear that only one structure per cell is found, independently of system size. For density $\rho = 0.08$ fm^{-3}, the same structure (cylindrical bubble) is observed for the three sizes, but for density $\rho = 0.04$ fm^{-3}, however, the smallest system forms a single punctured slab (PSlab) with a single hole (as the SSP did for that density), whereas the larger systems form a single regular slab. A suggestively

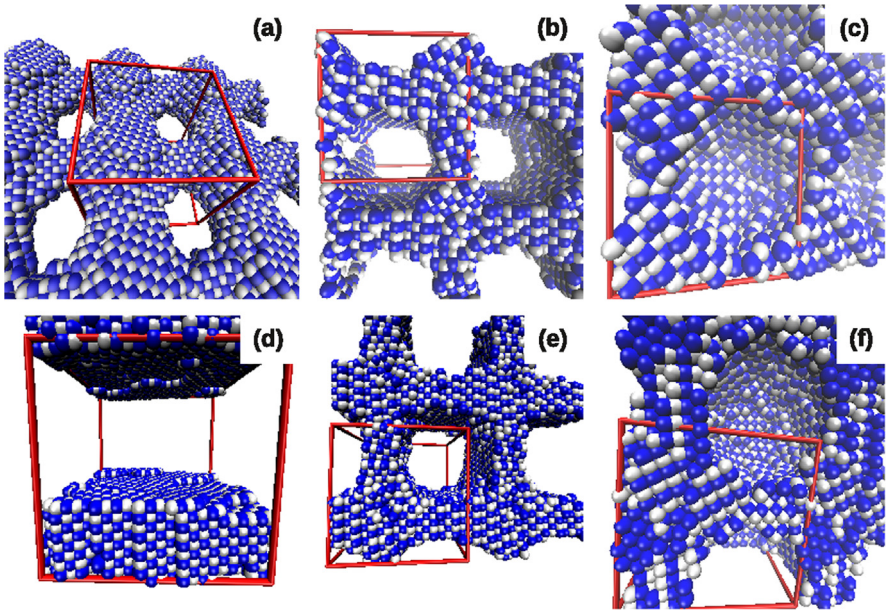


Fig. 14. (Color online.) Comparison of structures for the Pandharipande medium potential with $A = 1728$ (top row) and $A = 4096$ (bottom row) for densities $\rho = 0.04$ fm^{-3} (panels (a) and (d)), $\rho = 0.08$ fm^{-3} (panels (b) and (e)) and $\rho = 0.1$ fm^{-3} (panels (c) and (f)).

similar situation was observed by Williams and Koonin [6] who reported a "slab with regular holes". However, they found only one such hole per cell so the apparent "regularity" of the holes is caused by the periodic boundary conditions and not physical. In their work, they state that such structure appears to be the minimum energy configuration at a very small range of densities between a "rod" and a "slab", and that it becomes a slab by adiabatically increasing the density in a larger cell. This scenario is compatible with our own findings.

To estimate the surface area of this structure we approximate it by a slab with a cylindrical hole. To parametrize it, it is necessary to use the width of the slab (a), and the radius of the holes b as independent parameters. In terms of the volume fraction u it is

$$b = \frac{L}{\sqrt{\pi}} \times \sqrt{1 - \frac{L \times u}{a}},$$

$$S_{Pslab} = 2L^2 \times \frac{L \times u}{a} + 2\pi b \times a.$$

As shown in Fig. 15, the punctured slab is never the minimum surface shape among those structures considered. Furthermore, the total surface area of the punctured slab does not scale with L^2 as all the others. The leading term actually scales as L^3/a which is always larger than L^2, so for larger values of L this shape will always have a larger surface than the other shapes considered; yet our simulations yielded one. This may happen because small cells yield slabs so thin that the particles at one surface could interact with those at the opposite surface; such effect would occur in slab with thicknesses comparable to twice the range of the interaction. In such case higher order energy terms may become relevant. This seems to be the case in Fig. 14, since the punctured slab has a maximum breadth of $\sim$20 fm and a minimum of $\sim$10 fm, while the

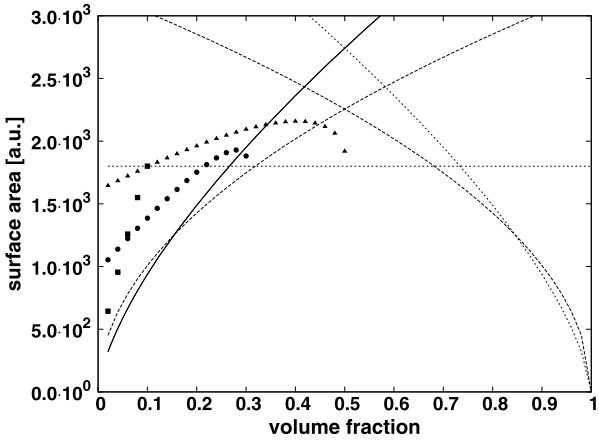


Fig. 15. Surface area of punctured slabs of width $w = 0.25L$ (squares), $w = 0.55L$ (circles) and $w = 0.85L$ (triangles) for $L = 30$. Surface area of other shapes are included for comparison: sphere and spherical bubble (dotted line), rod and cylindrical tube (dashed line) and slab (full line).

potential has a range of $r_c = 5.4$ fm. The regular slab with $A = 4096$ has a constant width of $\sim$16 fm. For $A = 1728$ and $\rho = 0.05$ fm^{-3}, the cubic cell's length is 32.6 fm, while the range of the potential is $r_c = 5.4$ fm. That is, the cell is only 6 times the range of the potential, hence it is possible that interfacial or curvature effects might be of the same order than surface effects.

The energy difference between the full slab and the punctured slab is so small that, as Williams and Koonin stated in [6], it would be "washed out" by finite temperature. This is a "small size" effect that can be avoided by using larger systems, but "finite size" effects are always present.

For the sake of argument, we show in Fig. 16 results obtained with $A = 13\,824$ and $A = 46\,656$ particles. At density $\rho = 0.05$ fm^{-3} we found slab-like structures for all system sizes equal or larger than $A = 4096$. For density $\rho = 0.08$ fm^{-3}, with $A = 13\,824$ almost cylindrical holes are observed, with some modulation. That modulation might be due to fast cooling. Incidentally, the slab for $A = 46\,656$ is stable at higher temperatures than for smaller systems. Compare, for example, Fig. 2 and Fig. 5: For $A = 1728$ the $T \sim 0$ MeV solution is a slab but becomes distorted at higher temperatures.

Results from this section indicate that the imposition of periodic boundary conditions is responsible for the formation of pasta-like structures in absence of Coulomb interaction rather than "finite size". In sight of this result, it is not so clear to which extent the imposition of periodic boundary conditions contribute to shape the results in Neutron Star matter simulations.

A rule of thumb to distinguish pseudo-pasta (i.e. that due to periodic boundary conditions) and "true" pasta (that arising form a balance between nuclear and Coulomb interactions) is that the scale of the pseudo-pasta structures is set exclusively by the size of the cell. This is evidenced by the fact that, without Coulomb interaction, there is systematically a single structure per cell. Any model that includes Coulomb interaction and aims to produce "true" pasta should, at least, be able to produce more than one structure per simulation cell.

5. Concluding remarks

Ideal nuclear matter was studied at sub-saturation densities and low temperatures using molecular dynamics with three different popular two-body potentials. Around saturation density,

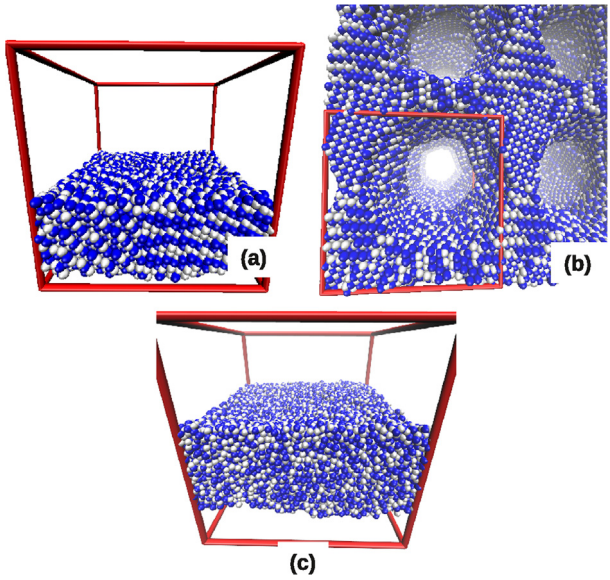


Fig. 16. (Color online.) Some results with larger systems. Panel (a) shows a $T = 0.001$ MeV configuration for $A = 13\,824$ at $\rho = 0.05$ fm^{-3}, (b) $T = 0.001$ MeV, $A = 13\,824$ and $\rho = 0.08$ fm^{-3}. Panel (c) shows a configuration for $A = 46\,656$ at $\rho = 0.05$ fm^{-3} and $T = 0.8$ MeV.

crystalline arrangements of the type simple cubic (B1), body centered cubic (B2) and diamond (B3) crystal lattices were to found. These lattice structures were produced by CMD in the temperature range of 0.001 MeV $\lesssim T \lesssim$ 1.0 MeV. A departure from the crystalline structure into non-homogeneous structures occurred whenever the density decreased below $\rho \approx 0.13$ fm^{-3}; this effect was observed at all temperatures below $T = 1$ MeV and for the three potentials.

At lower densities, where phase coexistence is expected at the thermodynamic limit, the matter arranged in non-homogeneous structures reminiscent of the usual pasta-like structures that have been observed in previous studies of Neutron Star Matter. The fact that these pseudo-pasta were formed without the Coulomb interaction (i.e. not through nuclear-Coulomb frustration) prompted a study of the role of the size cell and periodic boundary conditions on their formation. After demonstrating that pasta-like structures can be obtained even in a one-component Lennard-Jones system and that the volume energy played a minor role in the selection of the shapes, surface effects were investigated in turn. A simple geometric calculation showed that the use of periodic boundary conditions, rather than the size of the system, is responsible for the formation of these structures. These effects are not exclusive to this study nor to a particular interaction potential and we show them to be present in simulations with as much as 46 656 particles. This is explicit proof that the limit of very large systems $L \to \infty$ does not correspond, in general, to the thermodynamic limit as it is usually thought.

It has been addressed before [19] (and seems clear enough) that if a simulation of NSM yields a single structure per cell, it's likely to be biased by the finite size effects of the simulation, since the length scale of the structure is set by the artificial simulation cell rather than by a physically relevant competition between energy terms.

It is clear that the scenario with Coulomb interaction is rather different. The cause behind the fact that only one structure per cell arises in the systems studied in this work is that the simulation cell's finite size is the only thing preventing the "liquid" droplets from growing larger, as would

be thermodynamically favored at such densities. The size of the structures is only limited by the size of the cell, but the particular structures are shaped by the imposed periodicity. If Coulomb interaction were included, the competition between interactions of different ranges would lead to another characteristic length scale which would then physically limit the maximum size of the droplets. Thus, with Coulomb interaction, it is true that the effects of the periodic boundary conditions would vanish in the $L \to \infty$ limit. However, given that the shapes of the structures in both cases are the same, it is not clear to which extent the periodicity and symmetries imposed by the boundary conditions still affect the results of simulations even when Coulomb interaction is included. We believe that formation of non-homogeneous structures driven by surface minimization through artificial periodic boundary condition might still play a significant role in the simulations of NSM (i.e. with Coulomb interaction), specially at very low temperatures and at transition densities. And perhaps the fact that every reported pasta is a triply periodic minimal surface of cubic symmetry is related to the imposition of periodic boundary conditions of cubic symmetry.

These and other related issues will be tackled in an upcoming contribution.

Acknowledgements

C.O.D. thanks partial financial support by CONICET through Grant PIP0871, P.G.M. and J.I.N. are supported by CONICET scholarships, and J.A.L. by NSF-PHY Grant 1066031. C.O.D. and J.A.L. thank the hospitality of the Nuclear Theory Group of the Nuclear Science Division of The Lawrence Berkeley National Laboratory where this work was initiated.

References

[1] V.E. Viola, Nucl. Phys. A 734 (2004) 4879.
[2] D.Q. Lamb, J.M. Lattimer, C.J. Pethick, D.G. Ravenhall, Nucl. Phys. A 411 (1984) 449;
J.M. Lattimer, C.J. Pethick, D.G. Ravenhall, D.Q. Lamb, Nucl. Phys. A 432 (1985) 646;
J.M. Lattimer, C.J. Pethick, Astrophys. J. 223 (1978) 314.
[3] J.M. Lattimer, Annu. Rev. Nucl. Part. Sci. 31 (1981) 337.
[4] P. Bonche, D. Vautherin, Nucl. Phys. A 372 (1981) 496;
P. Bonche, S. Levit, D. Vautherin, Nucl. Phys. A 427 (1984) 278.
[5] D.G. Ravenhall, C.J. Pethick, J.R. Wilson, Phys. Rev. Lett. 50 (1983) 2066.
[6] R.D. Williams, S.E. Koonin, Nucl. Phys. A 435 (1985) 844.
[7] M. Hashimoto, H. Seki, M. Yamada, Prog. Theor. Phys. 71 (1984) 320.
[8] K. Oyamatsu, Nucl. Phys. A 561 (1993) 431.
[9] C.P. Lorenz, D.G. Ravenhall, C.J. Pethick, Phys. Rev. Lett. 70 (1993) 379.
[10] K.S. Cheng, C.C. Yao, Z.G. Dai, Phys. Rev. C 55 (1997) 2092.
[11] T. Maruyama, K. Niita, K. Oyamatsu, T. Maruyama, S. Chiba, A. Iwamoto, Phys. Rev. C 57 (1998) 655.
[12] T. Kido, T. Maruyama, K. Niita, S. Chiba, Nucl. Phys. A 663–664 (2000) 877.
[13] G. Watanabe, K. Iida, K. Sato, Nucl. Phys. A 676 (2000) 445.
[14] G. Watanabe, K. Sato, K. Yasuoka, T. Ebisuzaki, Phys. Rev. C 66 (2002) 012801(R).
[15] G. Watanabe, K. Iida, Phys. Rev. C 68 (2003) 045801.
[16] C.O. Dorso, P.A. Giménez Molinelli, J.A. López, in: C.A. Bertulani, J. Piekarewicz (Eds.), Neutron Star Crust, Nova Science Publishers, ISBN 978-1620819029, 2012.
[17] C.O. Dorso, P.A. Giménez Molinelli, J.A. López, Phys. Rev. C 86 (2012) 055805.
[18] C.J. Horowitz, M.A. Pérez-García, J. Piekarewicz, Phys. Rev. C 69 (2004) 045804.
[19] G. Watanabe, K. Sato, K. Yasuoka, T. Ebisuzaki, Phys. Rev. C 68 (2003) 035806.
[20] H. Pais, J.R. Stone, Phys. Rev. Lett. 109 (2012) 151101.
[21] W. Humphrey, A. Dalke, K. Schulten, VMD – visual molecular dynamics, J. Mol. Graph. 14 (1) (1996) 33–38.
[22] L. Wilets, E.M. Henley, M. Kraft, A.D. Mackellar, Nucl. Phys. A 282 (1977) 342.

[23] A. Vicentini, G. Jacucci, V.R. Pandharipande, Phys. Rev. C 31 (1985) 1783;
R.J. Lenk, V.R. Pandharipande, Phys. Rev. C 34 (1986) 177;
R.J. Lenk, T.J. Schlagel, V.R. Pandharipande, Phys. Rev. C 42 (1990) 372.
[24] C.O. Dorso, J. Randrup, Phys. Lett. B 215 (1988) 611.
[25] C.O. Dorso, S. Duarte, J. Randrup, Phys. Lett. B 188 (1987) 287–294.
[26] C.O. Dorso, J. Randrup, Phys. Lett. B 301 (1993) 328.
[27] C.J. Horowitz, M.A. Pérez-García, J. Carriere, D.K. Berry, J. Piekarewicz, Phys. Rev. C 70 (2004) 065806.
[28] C.J. Horowitz, M.A. Pérez-García, D.K. Berry, J. Piekarewicz, Phys. Rev. C 72 (2005) 035801.
[29] J. Piekarewicz, G. Toledo Sánchez, Phys. Rev. C 85 (2012) 015807.
[30] A. Chernomoretz, L. Gingras, Y. Larochelle, L. Beaulieu, R. Roy, C. St-Pierre, C.O. Dorso, Phys. Rev. C 65 (2002) 054613.
[31] A. Barrañón, C.O. Dorso, J.A. López, Nucl. Phys. A 791 (2007) 222.
[32] C.O. Dorso, J.A. López, Phys. Rev. C 64 (2001) 027602.
[33] C.O. Dorso, C.R. Escudero, M. Ison, J.A. López, Phys. Rev. C 73 (2006) 044601.
[34] C.O. Dorso, P.A. Giménez Molinelli, J.A. López, J. Phys. G, Nucl. Part. Phys. 38 (2011) 115101;
C.O. Dorso, P.A. Giménez Molinelli, J.A. López, Rev. Mex. Fis. 57 (1) (2011) 14.
[35] B.G. Todd-Rutel, J. Pieckarewicz, Phys. Rev. Lett. 95 (2005) 122501.
[36] U. Garg, Nucl. Phys. A 731 (2004) 3.
[37] G. Colo, et al., Phys. Rev. C 70 (2004) 024307.
[38] H.C. Andersen, J. Chem. Phys. 72 (1980) 2384.
[39] K. Binder, B.J. Block, P. Virnau, A. Tröster, Am. J. Phys. 80 (2012) 1099.
[40] D. Frenkel, B. Smit, Understanding Molecular Simulations, 2nd ed., Academic Press, 2012.